Emergent decoherence induced by quantum chaos in a many-body system: A Loschmidt echo observation through NMR

C. M. Sánchez [1] A. K. Chattah [1,2] and H. M. Pastawski [1,2,*]

[1]*Facultad de Matemática, Astronomía, Física y Computación, Universidad Nacional de Córdoba, 5000 Córdoba, Argentina*
[2]*Instituto de Física Enrique Gaviola (CONICET-UNC), 5000 Córdoba, Argentina*

In the long quest to identify and compensate the sources of decoherence in many-body systems far from the ground state, the varied family of Loschmidt echoes (LEs) became an invaluable tool in several experimental techniques. A LE involves a time-reversal procedure to assess the effect of perturbations in a quantum excitation dynamics. However, when addressing macroscopic systems one is repeatedly confronted with limitations that seem insurmountable. This led to the formulation of the *central hypothesis of irreversibility* stating that the timescale of decoherence, T_3, is proportional to the timescale of the many-body interactions we reversed, T_2. We test this by implementing two experimental schemes based on Floquet Hamiltonians where the effective strength of the dipolar spin-spin coupling, i.e., $1/T_2$, is reduced by a variable scale factor k. This extends the perturbation timescale, T_Σ, in relation to T_2. Strikingly, we observe the superposition of the normalized Loschmidt echoes for the bigger values of k. This manifests the dominance of the intrinsic dynamics over the perturbation factors, even when the Loschmidt echo is devised to reverse that intrinsic dynamics. Thus, in the limit where the reversible interactions dominate over perturbations, the LE decays within a timescale, $T_3 \approx T_2/R$ with $R = (0.15 \pm 0.01)$, confirming the emergence of a perturbation independent regime. These results support the central hypothesis of irreversibility.

I. INTRODUCTION

The last two decades have shown a growing interest on the understanding of how the classical limit [1], thermalization [2], and hydrodynamic behavior [3,4] emerge from quantum dynamics in closed many-body systems [5–10]. This interest is driven by new quantum technologies ranging from heterostructures to cold atoms, nitrogen vacancy and P1 centers in diamond, Bose-Einstein condensates, and a number of others [11–16]. All of them have quantum excitations, "particles," or qubits, the interactions of which can be manipulated periodically to engineer new forms of synthetic quantum matter away from its ground state. Such progress became concatenated with the demands of quantum information and computation, and a new theoretical and experimental drive on many-body quantum chaos (MBQC). This last became a condition to match quantum mechanics and gravity in the chaotic proximity of a black hole [17,18]. MBQC would ensure the fast scrambling of quantum information as characterized through out-of-time order (OTO) commutators that describe an exponential increase of quantum uncertainties. Such growth could be traced back to chaotic instabilities already present in single-particle dynamics [19,20]. Since the evaluation of these commutators requires OTO correlation functions (OTOCs) that involve a time-reversal procedure, Kitaev [21] and a number of authors [22–25] noted their equivalence with a family of experiments known as *Loschmidt echoes* (LEs) [26–28]. These implement time reversal through the sudden inversion of the Hamiltonian sign. Calculations and experiments in different systems confirmed the scrambling phenomenon and dubbed it the *quantum butterfly effect*, as initially localized information rapidly spreads and mixes under a Hamiltonian dynamics [29–33].

Nevertheless, these works have not addressed some related fundamental questions: To what degree do quantum-mechanical predictions, repeatedly tested on fairly small systems, remain valid when the number of involved particles increases substantially? Are hydrodynamic behavior and equilibration just an illusion due to the coarse grained measurement? Do the systems retain their memory of the initial state, i.e., the quantum correlations that encode it? Most physicists would give an emphatic affirmative answer. As an example, one could invoke the widely discussed black-hole information paradox [34] which, roughly, implies that the Hawking radiation of a black hole contains some of the information it had previously swallowed. However, our physical intuition, and even common wisdom [35], hints at the opposite view. We are more ready to admit that when a thermodynamic limit is applicable [36], i.e., the number of particles $N \to \infty$ and *then* the "friction" or energy uncertainty $\eta \to 0$, quantum dynamics could manifest a sort of phase transition as discussed by Anderson in his insightful paper "More is different" [37,38]. Thus, quantum mechanics would not be in question [39,40], but rather the flaw might be in how it is used. The limited availability of computational resources and analytical tools could hide a possible quantum dynamical phase transition towards intrinsic decoherence or irreversibility [37,38]. Our approach is to search

*horacio@famaf.unc.edu.ar

for answers to those questions using specifically planned experiments.

Once more, nuclear magnetic resonance (NMR) remains at hand as a well-developed toolbox to test the frontiers of quantum mechanics. Indeed, Feher's electron-nuclear double resonance on doped silicon yielded the puzzling evidence [41] that led Anderson to propose the "absence of spin diffusion" [36], the first quantum phase transition ever recognized [42]. More recently, NMR was used, following another hint of Anderson [43], to identify a quantum dynamical phase transition induced by a spin environment [6]. It also allowed the observation of quantum criticality [44,45] and signatures of many-body localization on spin dynamics [46,47]. Furthermore, a combination of magnetic resonance and optical techniques applied to impurities in diamond allowed a record in coherence time [48]. They also allow one to address the microscopic basis for spin diffusion [49,50] by observing, in real time, the emergence of the hydrodynamic behavior [3,4]. These works involved *dynamical decoupling* and other forms of LEs.. The first LE was introduced by Hahn [51] and Brewer and Hahn [52]. Their *spin echo* (SE) reverts the precession of individual spins, and is limited by T_2, the timescale of multispin interactions that scramble a local excitation in its neighborhood. Much later, *magic echoes* (MEs) achieved the recovery of that SE decay [53]. The related *multiple quantum coherences* (MQCs) [54] constitute an early NMR version of the OTOCs [31,55,56]. There, many-body time-reversal procedures are repeated to quantify the number of spins effectively coupled. A further step was the *polarization echo*, in which a *local* excitation was injected and observed to diffuse away before its partial recovery [26,57]. Simultaneously, we have learned to quantify the timescale T_Σ, that characterizes the experimental errors and noncontrolled interactions [58,59]. However, in spite of these impressive successes we face a fundamental limitation already encountered by our predecessors [60,61]: many-body time reversal fails lamentably already at rather short timescales. Further experiments consistently showed that the reversibility time, T_3, was just a few times longer than T_2 [26,55,59,62,63]. This seemed quite discouraging as this is the timescale of multispin interactions that one claims to control up to a reasonable precision of a few percent, i.e., $2\eta/\hbar \approx 1/T_\Sigma \ll 1/T_2$. Thus, reversibility timescale T_3 seems to be unavoidably tied to T_2. We should remark that all these solid-state NMR experiments involve a spin-lattice relaxation time $T_1 \gg \max(T_\Sigma, T_2)$, which ensures a fully quantum behavior. As $N \approx 10^{23}$, our system is already infinite to all practical purposes. Thus, the last step to take in the thermodynamic limit is to sweep the system from $T_\Sigma < T_2$ towards $T_\Sigma \gg T_2$. This is what we did by implementing a *multipulse scaled dipolar interaction* (MPSDI) sequence that yielded a value of T_3 consistent with an emergent property [56]. One might still wonder whether a lucky compensation of errors might have masked the improvement of the MPSDI sequence used to yield a universal scaling curve. This issue is what this paper brings under definitive scrutiny by developing quite robust new tools that combine novel [64] and traditional [65] techniques to scale down the natural interactions while keeping T_Σ constant.

With the stated purpose, we introduce two experimental procedures to measure the LEs, of the magic echo type, that use a *continuous wave scaled dipolar interaction* (CWSDI) either in the backward or in the forward evolution. Each of them allows one to change the relative importance of the Hamiltonian interactions with respect to the uncontrolled ones. This is achieved by an off-resonance irradiation that induces a Floquet effective Hamiltonian expressed as Magnus expansion. Its zeroth-order term will be the target effective Hamiltonian with a reduced coupling constant, while the higher-order terms constitute a perturbation [66,67]. More specifically, our experiments rely on a previous implementation [64,68] that showed how off-resonance continuous irradiation generates a scaled effective Hamiltonian and, in some cases, cancels it [59]. This becomes equivalent to multiplying the natural dipolar Hamiltonian by a scaling factor k in the forward or in the backward evolution periods during the time-reversal sequence, while the elapsed time is adapted to obtain the maximal echo condition. In many aspects, this procedure resembles the ME [65] with the additional versatility of the k factor. Our present experimental findings give further support to the central hypothesis of irreversibility [38] stating that, for unbounded systems at high temperature, there is an intrinsic irreversibility timescale T_3 proportional to the scrambling time T_2. As we will extensively discuss below, the LE decays as a logistic function, which is consistent with our hypothesis that MBQC drives a quantum dynamical phase transition towards an emergent intrinsic irreversibility.

II. ECHOES FOR THE SCALED DYNAMICS

The system is a polycrystalline sample of adamantane consisting in $N \approx 10^{23}$ nuclear spins-1/2, in presence of a strong magnetic field $\mathbf{B}_0 = B_0 \hat{z}$ that results in the Larmor frequency $\omega_0 = \gamma B_0$. At room temperatures, $k_B T \gg \hbar\omega_0$, the system is in a Boltzmann thermal state, described by the density operator $\rho(0) = I/D + \Delta\rho(0)$, with $\Delta\rho(0) \propto I^z = \sum_i I_i^z$ and D the dimension of the Hilbert space. As the identity does not evolve or give rise to a signal we will be concerned only with the deviation $\Delta\rho$.

The secular dipolar Hamiltonian with quantization axis z in the rotating frame is

$$\mathcal{H}_d^z = \sum_{i<j} d_{ij}\left(3 I_i^z I_j^z - \mathbf{I}_i \cdot \mathbf{I}_j\right)$$
$$= \sum_{i<j} d_{ij}\left(2 I_i^z I_j^z - \frac{1}{2}[I_i^+ I_j^- + I_i^- I_j^+]\right), \quad (1)$$

which in most theoretical papers is referred as XXZ. Here, the dipolar coupling strengths are $d_{ij} = (\mu_0/4\pi) \times (\gamma^2 \hbar) \times [1 - 3\cos^2(\vartheta_{ij})]/(2r_{ij}^3)$, the internuclear vector is $\mathbf{r}_{ij}$, and the angle between $\mathbf{r}_{ij}$ and the direction of the external magnetic field is ϑ_{ij} [69,70]. $I^\alpha = \sum_i I_i^\alpha$ (with $\alpha = x, y, z$) are the total spin operators. These interactions define the "spreading" timescale for the dipolar dynamics,

$$T_2 = \hbar/M_2 \quad \text{with} \quad M_2^2 = \text{Tr}[H_d^z, I^y]^2 / \text{Tr}[I^y I^y], \quad (2)$$

from the second moment of the Hamiltonian (from now on, $\hbar = 1$). After an initial pulse the system evolves, according to the details provided in the next section, under an effective Floquet Hamiltonian of the form $k_F \mathcal{H}_d^x$ during a forward time

t_F, and then under $-k_B \mathcal{H}_d^x$ during a backward time t_B. Thus,

$$\mathcal{H}_F = k_F \mathcal{H}_d^x + \Sigma_{k_F} \quad \text{and} \quad \mathcal{H}_B = -k_B \mathcal{H}_d^x + \Sigma_{k_B}. \quad (3)$$

The factors k_F and $-k_B$ modulate the natural dipolar Hamiltonian $\mathcal{H}_d^x$ in the quantization axis x, as presented in Refs. [64,68], and Σ_{k_F} and Σ_{k_B} account for experimental imperfections and high-order truncation errors resulting from the average Hamiltonian theory or can be neglected altogether depending on the case.

The propagator of the spin system at the end of experimental time $t = t_F + t_B$ has the form

$$\mathcal{U}_{LE}(t) = \exp(-it_F \mathcal{H}_F) \exp(-it_B \mathcal{H}_B). \quad (4)$$

The NMR signal generated by the propagator of the form (4) after a final rotation pulse is

$$M(t) = \text{Tr}[\exp(it_B \mathcal{H}_B) \exp(it_F \mathcal{H}_F) I^z \exp(-it_F \mathcal{H}_F)$$
$$\times \exp(-it_B \mathcal{H}_B) I^z] / \text{Tr}[I^z I^z]. \quad (5)$$

If one could neglect the perturbation terms Σ_{k_F} and Σ_{k_B} one would have a recovered signal:

$$M(t) = \text{Tr}\big(\exp\big\{\big[i\mathcal{H}_d^x(t_F k_F - t_B k_B)\big]\big\} I^z$$
$$\times \exp\big[i\mathcal{H}_d^x(t_B k_B - t_F k_F)\big] I^z\big\} / \text{Tr}[I^z I^z]. \quad (6)$$

The Loschmidt echo is obtained when the backward dynamics completely reverses the forward evolution, i.e., $\Sigma_{k_F} = \Sigma_{k_B} = 0$. The condition to be satisfied is

$$k_F t_F - k_B t_B = 0. \quad (7)$$

Only in this case the signal would result in the ideal condition where Σ_{k_F} and Σ_{k_B} are both identically zero, $M(t) \equiv 1$. As the previous condition is not perfectly given in experimental procedures, the measurement of $M(t)$, i.e., the LE intensity, quantifies the effectiveness of the reversion process and gives insights on the contributions of Σ_{k_F} and Σ_{k_B} to decoherence. Then, the LE decay allows us to define a "decoherence" timescale T_3^k, as the time at which the LE is one-half, $M(T_3^k) = 1/2$, that quantifies the time-reversal imperfections in the presence of the decoherent processes [56,71].

A. Scaling the Hamiltonian

To achieve the desired scaling factor k, we recall our experimental development described in Refs. [64,68]. The procedure involves the irradiation with a rf field in the off-resonance condition, that is, there is a difference between the Larmor and the rf frequencies. Here, $\Omega = \gamma b_0 = \omega_0 - \omega$ accounts for the off-resonance, where ω is the frequency of the rf field, which is applied with an intensity given by $\omega_1 = \gamma B_1$ (in rad/s). The secular Hamiltonian in terms of the effective frequency $\omega_e = \sqrt{\omega_1^2 + \Omega^2}$, in the *tilted frame* (X, Y, Z), is

$$\mathcal{H}_0^Z = -\omega_e I^Z + k_\theta \mathcal{H}_d^Z. \quad (8)$$

This (X, Y, Z) frame has the Z axis pointing in the direction of the effective field $\mathbf{B}_e = b_0 \hat{z} + B_1 \hat{x}$ that forms an angle θ with $\mathbf{B}_0$ [68,69]. The angle θ determines the value of the scale factor k_θ:

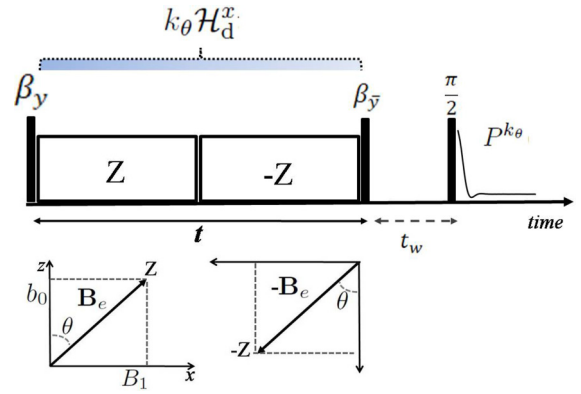$$k_\theta = \tfrac{1}{2}(3\cos^2\theta - 1). \quad (9)$$

FIG. 1. Experimental implementation to observe the polarization $P^{k_\theta}(t)$ under the scaled dipolar Hamiltonian evolution. Schematically, the lower panel shows the directions of the magnetic fields involved in the pulse sequence (irradiation, off-resonance, and effective). Each block irradiation time is incremented in multiples of the stroboscopic Floquet time $\tau_e = 2\pi/\omega_e$.

This factor can be varied experimentally by controlling the rf intensity ω_1 and the off-resonance Ω. Note that k_θ can vary continuously from 1 to $-1/2$, when θ ranges from zero to $\pi/2$ [64]. The special case $k_\theta = 0$ is achieved for the magic angle θ_m given by $\cos^2\theta_m = 1/3$, leading to an average decoupling in that condition. To observe the spin dynamics under the *scaled* dipolar Hamiltonian, $k_\theta \mathcal{H}_d$ during a time t, we implement two successive blocks of off-resonance rf irradiation with effective axis $\pm Z$, surrounded by hard pulses $(\beta)_{\bar{y}}$ and $(\beta)_y$, fulfilling $|\beta| = 90° - \theta$ (see Fig. 1).

Each block of duration $t/2$, a multiple of the Floquet time $\tau_e = 2\pi/\omega_e$, is described by a Hamiltonian shown in Eq. (8). The inversion in the phase and off-resonance of the rf field between the first and the second blocks swaps the direction Z to $-Z$, leading to the reversion of the Zeeman evolution, $\pm \omega_e I^Z$. The effect of the $\pm \beta$ pulses is to produce a global rotation onto the x axis, yielding a propagator governed only by the dipolar term,

$$\mathcal{U}_{k_\theta}(t) = \exp\left(-ik_\theta \mathcal{H}_d^x t\right), \quad (10)$$

where $\mathcal{H}_d^x$ represents the dipolar Hamiltonian with the quantization axis aligned with x axis of the rotating frame. The evolution of the thermal state I^z under the scaled Hamiltonian can be obtained as the signal measured by the sequence in Fig. 1:

$$P^{k_\theta}(t) = \text{Tr}\big[\mathcal{U}_{k_\theta}^\dagger(t) I^z \mathcal{U}_{k_\theta}(t) I^z\big] / \text{Tr}[I^z I^z]. \quad (11)$$

The name k_F denotes the value of k_θ when the irradiation angles satisfy $0 \leqslant \theta \leqslant \theta_m$, leading to a positive scaling factor in front of the dipolar Hamiltonian in the range [0,1]. For irradiation angles $\theta_m \leqslant \theta \leqslant \pi/2$, we denote $k_B = |k_\theta|$, leading to scaling factors k_B in the range [0, 1/2] and adding a minus sign in the backward Hamiltonian. In the following the subindex θ will not appear, understanding that for a given scaling factor the corresponding θ angle is set experimentally. Note also that the extreme case $\theta = 0$ with scaling factor $k_F = 1$ corresponds to the natural dipolar Hamiltonian (pulses in scheme 1, Fig. 2), while the opposite extreme case $\theta = \pi/2$ leads to a minus dipolar Hamiltonian with $k_B = 1/2$ and a
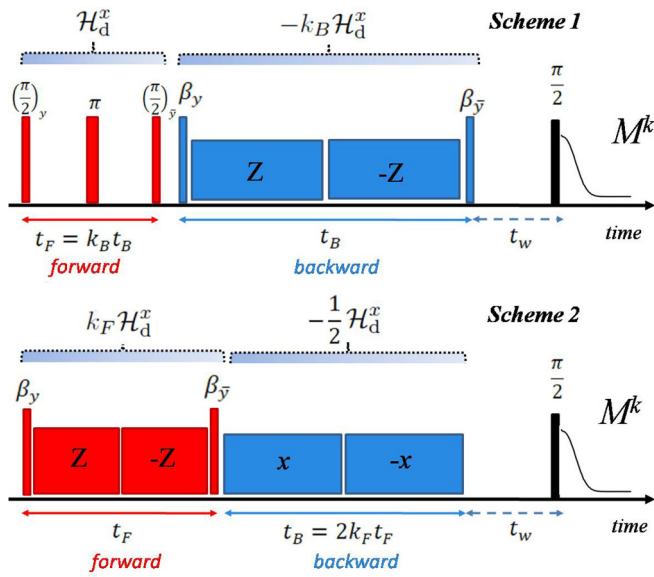
FIG. 2. Two experimental rf pulse sequences for the observation of the Loschmidt echo $M^k(t_e)$. The forward evolution was marked with t_F while backward evolution was marked with t_B. Each block of irradiation was incremented in multiples of the Floquet time $\tau_e = 2\pi/\omega_e$. Scheme 1: Forward dynamics is set to $k_F = 1$ and backward dynamics is given by $-k_B \mathcal{H}_d^x$ for k_B in the interval [0,0.5]. Scheme 2: Forward evolution is given by $k_F \mathcal{H}_d^x$ for k_F in the interval [0,1], and backward evolution is set with on-resonance irradiation $k_B = 1/2$. The variable scale factor in scheme 1 is k_B, while in scheme 2 it is k_F.

$Z = x$ quantization axis (on-resonance irradiation), schematized in Fig. 2, with $\pm x$ blocks of scheme 2 [53,65]. Both extreme cases do not involve off-resonance irradiation, which means less experimental error when implementing them.

B. Two complementary schemes for the echoes

We introduced the modulation of the dipolar dynamics with scaling factors k in Ref. [68], with the purpose to evaluate the corresponding LE decay, in a protocol dubbed *proportionally refocused Loschmidt* (PRL) *echo*. That sequence used two CWSDIs with identical factors k in the corresponding forward and backward blocks. While the PRL echo allowed us to evaluate MQCs and OTOCs [64], the concatenation of the two CWSDIs showed uncontrolled limitations in the matching of the off-resonance frequencies that prevented us from a confident comparison of the LE timescales for different k.

In the present paper we introduce two different schemes for the LE implementation (see Fig. 2) based on a single CWSDI dynamics. Each of them serves as a test that rules out possible errors of the LE from a MPSDI dynamics. Additionally, they yield a better time resolution of the dynamics with much shorter Floquet time. Both schemes also supersede the limitations previously encountered with the PRL echo sequence. In scheme 1 the forward evolution remains fixed as the natural dipolar one, not scaled $k_F = 1$, and thus has a negligible truncation error. The backward evolution is given by $-k_B \mathcal{H}_d^x$ for different choices of the value of k_B ranging in the interval (0,0.5). The forward time is adapted to meet the condition $t_F = k_B t_B$. In scheme 2, the forward evolution is given by

$k_F \mathcal{H}_d^x$ for different choices of the value of k_F belonging to the interval (0,1) while the backward evolution is implemented through on-resonance irradiation, which results in a fixed $k_B = 1/2$ and involves truncation errors of the order b^2/ω_1. In this case the backward time is adapted to meet the condition $t_B = 2k_F t_F$. As the scaling factor can be varied in a wider range, we can explore further possibilities than in the previous experimental conditions where we used strictly identical scaling and time for the forward and backward dynamics [56,68]. Both schemes can be considered as generalized ME pulse sequences, in which time-reversal protocols adapt forward and backward times. Indeed magic echo (forward dynamics with a full dipolar Hamiltonian and backward dynamics with half of the dipolar interaction achieved through on-resonance irradiation) is reproduced in the extreme value $k_B = 1/2$ for scheme 1. The nature of the scaling factors, however, allows us to explore different ratios between the controlled many-body dynamics and experimental (or truncation) errors. For these last we are able to obtain a clear experimental bound by studying the LE decay for many-body dynamics when the quantization frame rotates very close to the magic angle.

In each scheme, the Hamiltonian of interest is the one associated to the variable scale factor, backward in scheme 1 and forward in scheme 2. Then, the discussion refers to the scale factor $k = k_B$ or k_F in scheme 1 or 2, respectively. As time evolves, the scaled dipolar interaction connects the spin system entangling the quantum state with an increasingly complex character. This evolution time results in $t_e = t_B$ in scheme 1 and $t_e = t_F$ in scheme 2. Then, Loschmidt echo $M^k(t_e)$ is analyzed in terms of the scale factor k.

Note that both schemes are the same in the case $k = 0$ (evolution without average dipolar dynamic), where the adapted time results in zero in both cases, that is, $t_F = k_B t_B = 0$ for scheme 1 and $t_B = 2k_F t_F = 0$ in scheme 2. Then, when $k = 0$ the LE coincides with the measurement of the forward and backward dynamics, $M^{k=0} = P^{k=0}$.

C. Experimental procedure

The experiments were performed in a Bruker Avance II spectrometer operating at 300-MHz Larmor frequency, with a $\pi/2$ pulse time set at 4 μs. The sample temperature was controlled throughout the experiments at 303 K. Additionally, we did not observe appreciable heating effects produced by the continuous rf irradiation.

Previous settings were carried out to obtain the desired behavior in the different parts of the Loschmidt echo pulse sequence. Important care was focused on setting the rf irradiation fields and off-resonances to achieve accurately the same effective field frequency $\omega_e/2\pi = 79.8 \pm 0.2$ kHz for all k factors. By fixing $\omega_e = \sqrt{\omega_1^2 + \Omega^2}$ and k through $\frac{2k+1}{3} = \cos^2\theta = \frac{\Omega^2}{\omega_1^2 + \Omega^2}$ the experimental parameters ω_1 and Ω were calculated for each k as

$$\omega_1 = \omega_e \sqrt{\frac{1-2k}{3}}, \qquad (12)$$

$$\Omega = \omega_e \sqrt{\frac{2(k+1)}{3}}. \qquad (13)$$

Corrections to these values were obtained by performing off-resonance nutations, for each ω_1 and Ω, to obtain the desired effective frequency. Indeed for a given k the pure scaled Hamiltonian dynamics is obtained by implementing two consecutive blocks of rf pulses with opposite phases as depicted in Fig. 1. This procedure has the objective of refocusing nondesired evolution with the effective Zeeman Hamiltonian in the tilted frame (i.e., $\propto \omega_e I^Z$) and attenuating the effects of the rf inhomogeneity. Then special attention has been put on experimentally setting the $\pm\Omega$ values to obtain the desired performance. In particular, rf power ranged between 20 and 79 kHz, while the off-resonance took values up to 77 kHz. Duration of β pulses to rotate the quantization axis ranged between 0.70 and 3.36 μs. In all cases, the waiting time before the lecture pulse was set to $t_w = 0.5$ ms, to allow unwanted transverse magnetization to decay.

Forward and backward dynamics were evaluated for factors $\pm k$, including $k = 0$. Each block of irradiation was incremented in multiples of $\tau_e = 12.53$ μs to be consistent with the average Hamiltonian theory [68], producing evolution times, in the range 25.06 μs to 1.9 ms.

Schemes 1 and 2 for quantifying Loschmidt echo were successfully implemented for the different $\pm k$ values. In scheme 1, the backward Hamiltonian was scaled by factors $k = k_B = 0.05, 0.1, 0.15, 0.2, 0.25, 0.3, 0.35, 0.4, 0.45,$ and 0.5, where the special case $k_B = 0.5$ corresponds to the magic echo [51]. In scheme 2, the forward Hamiltonian was scaled by factors $k = k_F = 0.1, 0.2, 0.3, 0.4, 0.5, 0.6, 0.7, 0.8,$ and 0.9. In this case, scaling factors are strictly less than 1, $k_F < 1$. For both schemes the experimental times were adapted in order to fulfill Eq. (7).

III. DECAY RATES OF THE SCALED DYNAMICS

The transverse magnetization, $I^y(t)$, under the secular dipolar $\mathcal{H}_d^z$ (XXZ) is obtained by measuring the free induction decay (FID) after a $\pi/2$ pulse. In molecular solids such as adamantane, this magnetization follows a dynamics that fits a well-known model [72], the Abragam function:

$$P(t) = \text{sinc}(wt)\exp[-(ht)^2/2], \quad (14)$$

which captures both the decay and the damped oscillation arising from the unitary dynamics. The spreading timescale, Eq. (2), and the second moment of the Hamiltonian, $M_2 = (1/T_2)^2$, can be evaluated from the fitted parameters, $1/T_2 = \sqrt{h^2 + w^2/3}$.

The magnetization dynamics under the scaled Hamiltonian was investigated by applying the protocol of Fig. 1. The average Hamiltonian was quenched to $k_\theta \mathcal{H}_d^x$ and the total polarization as a function of the experimental time $I^z(t)$ [as expressed in Eq. (11)] was measured by recording the FID after $\pi/2$ pulse. We explored the behavior of $P^{k_\theta}(t)$ for various values of k_θ in the range $[-0.5, 1)$. One extreme of the interval, $k_\theta = -0.5$, is achieved through on-resonance irradiation ($\pm x$ blocks in scheme 2, Fig. 2). The limiting value $k_\theta = 1$ is the free evolution under the secular dipolar Hamiltonian pulses of scheme 1 in Fig. 2, without continuous irradiation.

Figure 3 displays, for example, the experimental points for $P^{k=0.25}(t)$ together with the fitting to Eq. (14). The lower panel of the same figure contains the values of $1/T_2^k$ vs k_θ, obtained
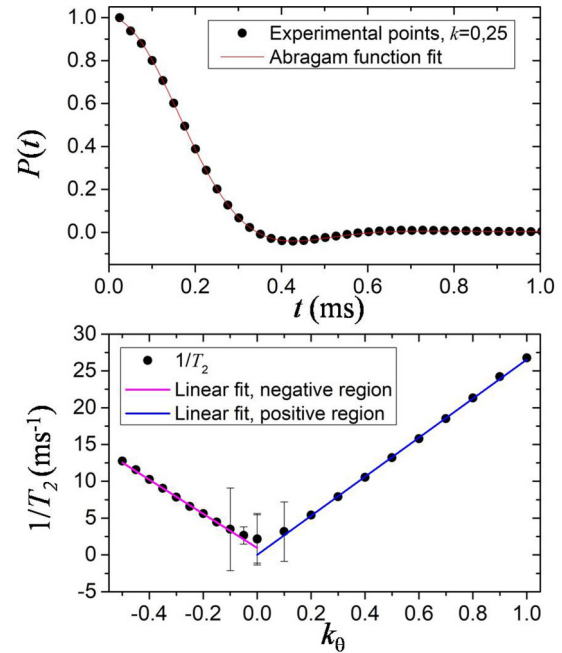

FIG. 3. Upper panel: Experimental data of $P(t)$ and fitting to Eq. (14) for $k_\theta = -0.25$. Lower panel: $1/T_2$ obtained from the fittings to Eq. (14) for positive and negative values of k_θ in the range $[-0.5, 1]$. Linear fittings for both regions show the good performance of the pulse sequence of Fig. 1.

from the fittings of $P^{k_\theta}(t)$ to Eq. (14). We observed a linear tendency of $1/T_2$ vs k_θ. Two different linear fittings for the positive and negative values of k_θ were performed. The slopes were 23.0 ms^{-1} for $k_\theta > 0$ and 26.5 ms^{-1} for $k_\theta < 0$. These linear curves confirm that the pulse sequence of Fig. 1 has a very good performance in scaling the dipolar Hamiltonian. Indeed for positive scale factors the interception of the linear curve with the ordinates is at the origin, while for negative scale factors this value is 1 ms^{-1}. The second moment of the scaled Hamiltonian is proportional to k as expected, showing also the accuracy of the experimental value of k obtained. The difference of 15% in both slopes indicates experimental errors in the implementation leading to a small difference to obtain positive and negative values of a given scale factor. For negative values of k the interception with the y axis is not at zero. This means that there is some remaining dipolar evolution while approaching to $k = 0$ from the negative side.

The inverse of the spreading times, $1/T_2^k$, is used in the following sections to analyze the behavior of decoherence vs dynamics.

IV. LOSCHMIDT ECHOES

The behavior of $M^k(t_e)$ divided by its maximum value as a function of t_e can be observed in Fig. 4, showing a monotonic slower decay as the k factor diminishes. This behavior has been observed with another experimental setup that produced a scaled dipolar Hamiltonian [56]. From these curves, the values of the decoherence times T_3^k were obtained as the half-height time, $M^k(T_3^k) = M^k(0)/2$. Indeed, $M^k(t_e)$ curves
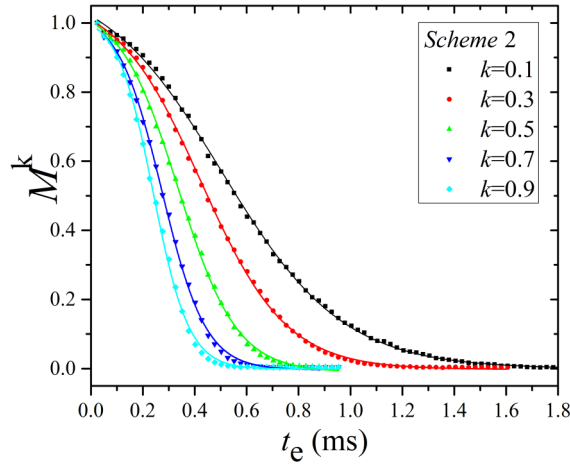
FIG. 4. Loschmidt echoes for selected values of the scaling factor, $M^k(t_e)$. The plot displays the experimental points normalized to the maximum value (dots), and the fittings to a logistic sigmoid function (lines). T_3^k were extracted from $M^k(T_3^k) = M^k(0)/2$. The curves show a decay monotonically ordered with k.

follow a particular form of sigmoid, the logistic function (Fermi function), with behavior of the form

$$M(t_e) = C/\{1 + \exp[\lambda(t_e - T_3)]\} \quad \text{with} \quad C \approx 1. \quad (15)$$

For the parameters of our system the inflection of the sigmoid is roughly the half-height time $t_e = T_3$, and $M^k(0) = C/(1 + \exp[-\lambda T_3]) \approx 1$. From then on an exponential decay occurs, with an exponent $1/\lambda \propto T_2$, that can be associated with a Lyapunov behavior that persists as long as the signal-to-noise ratio is significant.

Figure 5 displays the normalized Loschmidt echoes obtained by implementing schemes 1 (upper panel) and 2 (lower panel). Both sets of curves were plotted as a function of the scaled (or proper) time $t_s = k t_e$. The scaling factors are in the range [0.1,0.45] for scheme 1 and in the range [0.2,0.9] for scheme 2. The natural choice for normalization should be the $k = 0$ evolution $M^0(t) = P^0(t)$. Nevertheless, the experimental implementation for $k = 0$ has identical forward and backward parts; in contrast, any nonzero k echo measurements have different irradiation for forward and backward parts. Then we have used for normalization the Loschmidt echo with the lowest nonzero value of k available for each scheme, with the practical effect of capturing better the basic underlying experimental errors in each procedure, that is, $M^{\text{ref}} = M^{0.05}$ and $M^{0.1}$ for schemes 1 and 2, respectively. The normalization was performed by dividing for the reference at each time, $M^k(t_e)/M^{\text{ref}}(t_e)$. Indeed, the reference curves give a measure for the "perturbation" timescale $M^{\text{ref}}(T_\Sigma) = M^{\text{ref}}(0)/2$. The normalized echoes are characterized by decays that are inherent to the coherent dynamics. This is evidenced by the superposition of the normalized Loschmidt echoes in a common curve for all values of k, when displaying them as a function of scaled time, as shown in Fig. 5. Significantly, the same figure exposes that some points of M^k/M^{ref} depart from the common behavior at given times that depend on k. This fact arises from the experimental errors that are accumulated differently for each k and the use of different times of M^{ref}. Thus, the smaller the k values, the longer experimental times
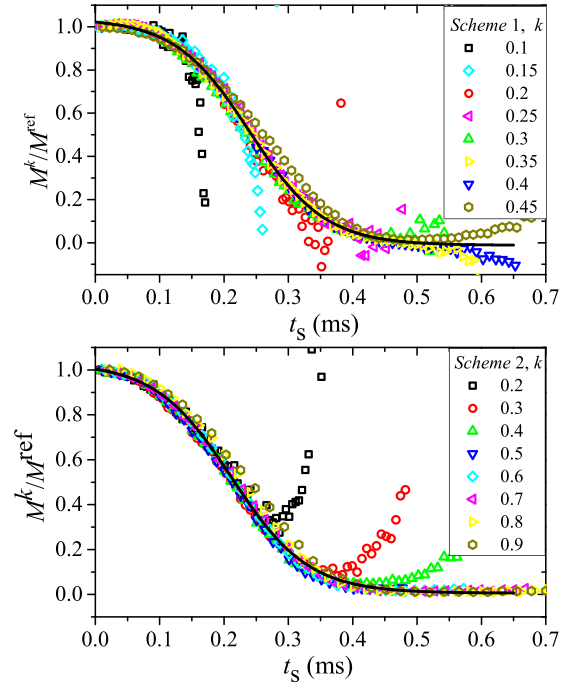

FIG. 5. Normalized Loschmidt echoes as a function of the scaled time, t_s. Upper panel: Scheme 1. Lower panel: Scheme 2. Continuous lines represent the logistic sigmoid fit.

t_e are needed to observe the echo at a given scaled time t_s. Then, there is a departure of the common behavior that occurs monotonically with k, that gives a limit for the reliability of the experiments as the signal fades within the statistical noise.

V. DECOHERENCE VS PERTURBATION

Figure 6 presents the behavior of decoherence rates $1/T_3^k$ in terms of the perturbation rate $1/T_\Sigma$, through dimensionless quantities obtained dividing by the spreading rate $1/T_2^k$. This exploration arises from the possibility to change the relative importance between coherent system dynamics and disturbance factors. The results derived from the scaling factors k implemented in each scheme were included in the figure, circles for scheme 1 and squares for scheme 2. As it was mentioned before, T_3^k is the inflexion point of the sigmoid fittings to $M^k(t_e)$ (see Fig. 4 curves), while T_2^k are derived from the Abragam fitting function $P^k(t)$, displayed in Fig. 3. Our evaluation of the perturbation rate $1/T_\Sigma$ deserves special mention. Our lower bounds for the times T_Σ were measured from the half-height time in the reference echoes M^{ref}, i.e., the LE when the Hamiltonian vanishes. The value of k selected for reference depends on the experimental implementation, as the smallest nonzero scale factor available for each scheme, that is, $k = 0.05$ for scheme 1 and $k = 0.1$ for scheme 2. At these angles the truncation error maximizes, while still having a nontrivial dynamics.

Figure 6 shows that the experimental data T_2^k/T_3^k vs $x = T_2^k/T_\Sigma$ follow a behavior of the form $\sqrt{A + x^2}$ in both schemes. Similar observation was found in Refs. [22,38]. The fitting parameter results are $A = (0.020 \pm 0.001)$ for scheme
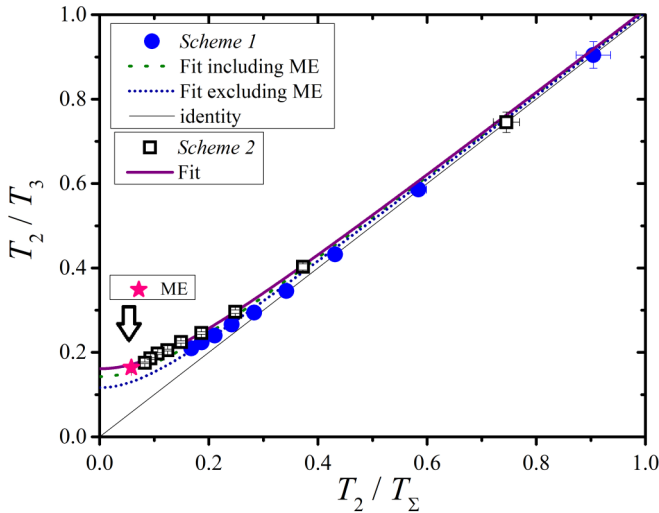
FIG. 6. Decoherence rates $1/T_3^k$ in terms of the perturbation rate $1/T_\Sigma$, both divided by the scrambling rates $1/T_2^k$. Experimental points belong to schemes 1 (circle) and 2 (square). A straight line with slope 1 shows the asymptotic behavior. Fittings to $\sqrt{A + x^2}$ were included for both schemes. Both schemes converge to the same ordinate T_2/T_3 at the origin, in spite of substantially different truncation errors in their natural Hamiltonian.

1 and $A = (0.026 \pm 0.001)$ for scheme 2. This means that in the zone of small k when $T_\Sigma \ll T_2^k$ the noncontrolled interactions dominate the intrinsic ones, and the experimental points fall on the line with unit slope, also shown in the figure. That is, for small k one has $T_3^k \approx T_\Sigma$. In this regime $M^{k=0}(t_e)$ shows an initial quadratic (Gaussian) decay that becomes an exponential indicative of Markovian processes [58,73], where the best fit is obtained with an *ad hoc* function proposed by Flambaum and Izrailev [74]. In the opposite extreme, there is a region where reversible dynamics is dominant, leading to an asymptotic tendency given by $T_2^k/T_3^k = \sqrt{A}$. Then, for scheme 1 the value $\sqrt{A} = (0.141 \pm 0.004)$ holds and for scheme 2 $\sqrt{A} = (0.161 \pm 0.003)$, leading, in the limit of vanishing perturbation, to the universal relation $T_2/T_3 \approx (0.15 \pm 0.01)$ that expresses the relation between the timescale of irreversibility in terms of T_2 and the intrinsic timescale at which the many-body effect manifests [75]. This value is common to both schemes, showing a universal tendency. At this point a maximum Lyapunov decay rate is reached at $1/\lambda = 1.7T_2$. The agreement with our previous work, where the MPSDI was implemented, is quite remarkable. As the experimental implementations of a scaled dipolar Hamiltonian are based on completely different principles, the magnitudes of the errors are also expected to be different. In all cases, the T_Σ's were evaluated through the decay of the Loschmidt echo for a nearly negligible dynamics [56], i.e., $(T_2/T_\Sigma)^2 \gg 1$. Thus, by varying k from 0 to 1 (or 1/2), the Loschmidt echo decay rate changes from the perturbation rate $1/T_\Sigma$ to the intrinsic irreversibility rate $1/T_3$, by passing through the decoherence rates. This is particularly true in scheme 1, since the truncation imposed by the Zeeman field is almost perfect, and decoherence occurs only during the scaled backward evolution. Remarkably, the lower k limit coincides for both schemes. Thus, the secular

dipolar interaction that yields the scrambling, in spite of being reversed by the LE, also determines the intrinsic irreversibility rate.

VI. CONNECTIONS WITH OTOCs AND QUANTUM CHAOS

A. How Loschmidt echoes provide a local observable

The local nature of the LE experiments was revealed by the *polarization echoes* [26,57], where a rare ^{13}C is a *local probe* that injects polarization in the directly bonded ^1H, i.e., through a SWAP gate [76]. It also detects the polarization diffused away through the ^1H network [77] in a timescale T_2. Since the excitation is a mixed state of *local* pseudopure states $I^y = \sum_n I_n^y(t)$, where each term evolves independently [78], one can focus on *one* of them, say I_0^y. A *forward* dynamics under a polarization conserving $\mathcal{H}$ is followed by the *backwards* one under $-(\mathcal{H} + \Sigma)$. The propagator $\mathcal{U}_{LE}(t)$ concatenates both, but only the many-body state that reconstructs the original I_0^y can transfer its polarization back to its ^{13}C neighbor. Thus, $M(t) = \text{Tr}[I_0^y \mathcal{U}_{LE}(t) I_0^y \mathcal{U}_{LE}^\dagger(t)]/\text{Tr}[I_0^y I_0^y]$. The quantum phase was confirmed by an interference between the returning amplitude and that remaining at ^{13}C, seen as high-frequency oscillations or *heteronuclear coherences* [26,79]. For many decades the *magic echo* seemed to yield a different physics than the *polarization echo*, because a *local probe is absent*. Moreover, the *polarization is not conserved*, but decays into multispin superposition, i.e., MQC [80]. Again, the initial state is a sum of independent pseudopure states as I_0^y. After time reversal, only that multispin component that reconstructs the *local* I_0^y produces an observable signal. Terms of polarization at sites other than zero have phases changing wildly with time, and interfere destructively during t_w. This effect is confirmed by numerical simulations [81,82]. Thus, all the experiments dealing with a reversed polarization that is not conserved—ME, MQCs or OTOCs, and PRL echoes—yield *local information*. This fact is crucial for our discussion.

B. How OTOCs and MQCs exploit LEs

In general, LE experiments have a *persistent* "perturbation" or Hamiltonian imprecision, Σ, during a whole period. In an ideal MQC (or the various OTOCs), the perturbation is just a *pulse*. Particularized by Swingle [83], an initial excitation, say $I_0^y = W$, evolves for a time t under the action of a noncommuting $\mathcal{H}$, producing a scrambled multispin superposition. Only then a "perturbation" Σ acts for a very a short period δt. A *time-reversed* evolution is imposed for a new period t, producing $\exp[-i\mathcal{H}t]VW(t)V^\dagger \exp[i\mathcal{H}t]$, used to evaluate an observable $W^\dagger$. In an NMR MQC experiment V is a global rotation $V = \exp[-iI^z\theta]$ [56], or a field gradient pulse [84]. Such perturbation labels with a phase θ_n the participation of a superposition state the total spin projection of which differs in n. Technically, one measures the total in-plane polarization $D = I^x$. However, as *only* the component of the multispin state that has returned to the original site, i.e., I_0^y, contributes to the observed signal, $M_\theta(t) = \text{Tr}[W^\dagger(t)V^\dagger(0)W(t)V(0)]$. This OTOC, if normalized properly, is 1 for $t = 0$ and then has a decay [18,19,21,56,85] related to the increase of $|[V(0), W(t)]|^2$. In a MQC

experiment, one uses the $M_\theta(t)$ dependence on θ to evaluate $|[I_0^y(t), I_0^y(0)]|^2$. This, in turn, encodes the number of spins that became entangled by the dynamics [21,54,56,86]. Time reversal is just a tool to evaluate the information scrambling. Some unavoidable errors or Hamiltonian imprecision Σ produce the signal decay without affecting the scrambling quantifier, i.e., the θ dependence, as one can always normalize with the LE, $M_\theta(t)/M_0(t)$, at a given time. In contrast with other OTOCs [87], MQCs do not depend on decoherence [88], as it is only limited to the time range with significant signal-to-noise ratio [89].

C. Quantum chaos as the dynamical instability under a perturbed time reversal

A first hint at the manifestation of a Lyapunov classical instability in the quantum realm came in the pioneering work of Larkin and Ovchinnikov [19] and Laughlin [20]. They considered a semiclassical wave packet with wavelength λ_F and velocity v_F that describes the conductivity of metals. The regime of "quantum chaos" [90,91] of short scattering time τ_o, as in a random array of antidots of size $a \gg \sqrt{\lambda_T v_F \tau_o}$, was loosely characterized by a single Lyapunov exponent λ, manifested through a diffusion coefficient $D \propto v_F^2/\lambda$, up to a logarithmic factor $\ln[v_F \tau_o/a]$. Thus, the exponential growth of an OTO commutator is a Lyapunov growth of quantum uncertainties, at least up to the Ehrenfest time $t_E = \lambda^{-1} |\ln[a/\lambda_F]|$, justifying the name "quantum butterfly effect" [24,83]. Nevertheless, the LE approach involved a radically new concept, since quantum dynamics of classically chaotic systems [92] and spin-1/2 systems [93] are stable towards changes in the initial conditions. The dynamical instability manifests under a steady perturbation [26,27,38,62]. For a weak perturbation, the LE decays with Fermi's "golden rule" in a time T_Σ. However, systems with a classically chaotic correspondence show a LE displaying an exponential decay with rate $1/T_3 = \min[1/T_\Sigma, \lambda]$, where λ is the Lyapunov exponent of the classical system. That is, above a small Σ_c, the classical and quantum LE decays coincide. Differently from an OTO commutator growth, this exponent still shows up *beyond* the Ehrenfest time [94,95]. For high energies Σ_c becomes negligible, which corresponds to the classical limit [91]. In many-spin systems, the lack of a classical counterpart prevents a direct extrapolation of these results. Nevertheless, high temperatures correspond to high energies and the perturbation independent decay is expected if Σ exceeds a small Σ_c. This is consistent with spectral and dynamical signatures of quantum chaos [2,96,97] shown by XXZ Hamiltonians. Our experimental LE decay, Eq. (15), was first found in Ref. [98]. It also appeared in the LE of hard disk gas [99], defined as the probability that one disk returns to its initial neighborhood under the effect of a weak perturbation. T_3 depends on the strength of the perturbation, while λ is the Lyapunov exponent [100]. Equation (15) was observed for LEs in interacting fermions and Bose-Einstein condensates [101]. Again, λ did not depend on the perturbation strength but on the Hamiltonian. Additionally, T_3 decreases with the logarithm of the perturbation or the system size, indicating an emergent behavior in the thermodynamic limit. These antecedents justify our identification of λ as a Lyapunov exponent.

VII. CONCLUSIONS: MANY-BODY QUANTUM CHAOS LEADING TO IRREVERSIBILITY

In the present paper we have been able to evaluate the LE irreversibility timescale T_3, by varying the ratio T_2/T_Σ between the timescale of the controlled many-body Hamiltonian and that associated with the Hamiltonian imperfections. These timescales are usually disguised, but scaling down the interaction allows its full disclosure as $T_2^k/T_3^k \rightarrow T_2^k/T_\Sigma$ as $k \rightarrow 0$ when $(T_2^k/T_\Sigma)^2 \gg 1$. In the opposite regime, $(T_2^k/T_\Sigma)^2 \ll 1$, we approach the thermodynamic limit, and the asymptotic perturbation independent T_3 manifests the emergence of an *intrinsic irreversibility* in the many-body dynamics. The quantum chaos is expressed in the LE exponential decay when irreversibility becomes intrinsic, $T_3 \simeq 6.7 T_2$. Since the perturbations are local, one needs the development of nonlocal superposition states before the intrinsic decoherence arises [102]. From then on, the LE decays exponentially with $\lambda^{-1} \simeq 1.7 T_2 = 0.25 T_3$, which can be identified as a Lyapunov time. This situation confirms the validity of the results observed with the MPSDI sequence [56], where the nature and strength of the perturbation are different from those that appear here. This indicates a universal characteristic of the XXZ Hamiltonians. Also the fact that schemes 1 and 2 coincide definitely rules out the possibility that the truncation of the Hamiltonian could be the main source of irreversibility observed in the various forms of Loschmidt echoes. This is because, while in scheme 2 the truncation of the backward evolution is the result of the limited rf strength, in scheme 1 the decoherent perturbations are limited only to the backward CWSDI portion. Furthermore, our present results are decisive to conclude that the scaling function is not based on an experimental artifact of the MPSDI sequences. On the basis of this, we may recommend the evaluation of T_3 by using any of the variants of MPSDI for the backward dynamics, together with a forward part in absence of irradiation. Additionally, MPSDI could be used in biological systems without the risk of heating.

We recall that we have also implemented a Floquet double quantum (DQ) Hamiltonian in the same crystal, obtaining $\lambda^{-1} \approx 0.23 T_3$. In that case the scrambling is much faster and the number of entangled spins grows exponentially [46,103] instead of diffusively as occurs for XXZ [56,64]. The "ballistic" behavior of the DQ is more clear in a linear topology [98], showing a wavefront propagating as prescribed by the Lieb-Robinson bound [79,104–106]. The dependence of the DQ dynamics on perturbation has not yet been reported, but a multiple pulse implementation is in progress. However, this more reversible dynamics manifests in fact that the signal only fades away after reaching 10^4 entangled spins [46,64], which largely exceeds the 10^2 of the dipolar case. We also may compare our present results with the LE of the polarization echo type under an XXZ Hamiltonian. There, the LE decay remains Gaussian as long as the signal-to-noise ratio is significant. In this case, different experiments with a number of ratios between the Hamiltonian and perturbation strengths hint at an emergent T_3 of about $4 T_2$ [38,58,62]. As a whole, these results show that the specific decay laws and their proportionality factors depend on the particularities of the system, like the topology of interactions network, on

the specific Floquet effective Hamiltonian, and of course on the nature of the excitation. Thus, in spite of numerical support [100,101], one should be careful not to attribute excessive universality to the observed decay laws. It is beyond the scope of our present paper to rule out the existence of integrable many-body systems that manifest a perturbation independent irreversibility. Nevertheless, we accumulated two decades of experimental and theoretical antecedents on spin systems far from equilibrium in regimes that can be identified as many-body quantum chaos. Their general feature is that a small, but global, perturbation is amplified to allow the full irreversibility. The irreversibility timescale, while proportional to the spreading time, is an intrinsic property of the experiment.

On the conceptual side, our experiments may inspire specific procedures to store and spread information. The understanding of the timescales involved could prevent strategies doomed to failure in favor of more viable alternatives. It is now clear that the original magic echoes experiments were already done in a nearly optimal regime where errors were small enough. This sets the echo decay in the perturbation independent regime, where the central hypothesis of irreversibility holds. Thus, there was not much room to improve the magic echo reversibility as its decay was determined by the intrinsic chaotic instability of the many-body system. This explains the failure of the long quest of Waugh to improve the magic echo experiments [52,61]. In contrast, the initial flat region of the Loschmidt echo opens the possibility to apply quantum error correction protocols while they are still effective [107], which seems consistent with the announced plans to use over 1×10^6 qubits to control the performance of 100 qubits [108].

On a more fundamental aspect, our experiments cannot represent a valid model of a quantum system that satisfies the AdS-CFT correspondence. This is because the Lyapunov exponent we found, $\lambda \propto d/\hbar \ll k_B T/\hbar$, is too small to satisfy the Maldacena bound [18] of $\lambda \lesssim k_B T/\hbar$. This quite exceptional condition is satisfied by the Sachdev-Ye-Kitaev model, especially devised with this purpose [21], but not by our XXZ Hamiltonians. Nevertheless, our results could provide a solution to the black-hole information paradox and to the origin of the arrow of time. Indeed, we perceive time to move only towards the future. Yet, quantum dynamics, like other basic laws of physics, works equally well forward or backward in time.

How is this apparent contradiction solved? The more accepted view is that to account for it we have to delve into the initial conditions after the big bang. Indeed, Maldacena noted that "a black hole singularity is somewhat similar to the singularity at the beginning of the Universe, just it is time reversed" [34]. This analysis seems reinforced by the new experiments that found that time reversal is not affected by chaos, interpreted as *the quantum butterfly noneffect* [109,110]. There, the authors implement a sequence of operations on a qubit that could be equivalent to classical chaos. The OTOC of the quantum version, implemented in a five qubit IBM quantum processor, showed a fine stability towards changes in the initial condition. Indeed, there is no problem with these results, which are consistent with our early predictions for one-body quantum chaos [27,94]. Our present experiments, in contrast, consider a huge number of interacting qubits, of which a few hundred become entangled. However, errors, though quite small, act at every time step. The fact that we find an intrinsic irreversibility or decoherence time adds evidence in favor of the idea that an actual chaotic many-body system far from its ground state contains irreversibility as an emergent property of the thermodynamic limit. The importance of such a result needs further validation that is beyond present computational possibilities. As Feynman pointed out, the most immediate task for quantum computers is to simulate quantum systems [111,112]. Since this is not foreseen as an easy task, it might challenge researchers that master other quantum information techniques to implement simulators of many-body LEs. These should focus on models, probably similar to our XXZ Hamiltonian, that could test the emergence of intrinsic irreversibility in the thermodynamic limit.

[1] W. H. Zurek, Rev. Mod. Phys. **75**, 715 (2003).

[2] F. Borgonovi, F. M. Izrailev, L. F. Santos, and V. G. Zelevinsky, Phys. Rep. **626**, 1 (2016).

[3] D. Pagliero, P. R. Zangara, J. Henshaw, A. Ajoy, R. H. Acosta, J. A. Reimer, A. Pines, and C. A. Meriles, Sci. Adv. **6**, eaaz6986 (2020).

[4] C. Zu, F. Machado, B. Ye, S. Choi, B. Kobrin, T. Mittiga, S. Hsieh, P. Bhattacharyya, M. Markham, D. Twitchen *et al.*, Nature **597**, 45 (2021).

[5] S. Popescu, A. J. Short, and A. Winter, Nat. Phys. **2**, 754 (2006).

[6] G. A. Álvarez, E. P. Danieli, P. R. Levstein, and H. M. Pastawski, Phys. Rev. Lett. **101**, 120503 (2008).

[7] C. Gogolin and J. Eisert, Rep. Prog. Phys. **79**, 056001 (2016).

[8] Y. Aharonov, S. Popescu, and D. Rohrlich, Proc. Natl. Acad. Sci. USA **118**, e1921529118 (2021).

[9] J. L. Lebowitz, IAMP News Bulletin 4 (2021), http://www.iamp.org/bulletins/Bulletin-Apr2021-print.pdf.

[10] J. L. Lebowitz, Phys. Today **46**, 32 (1993).

[11] J.-Y. Choi, S. Hild, J. Zeiher, P. Schauß, A. Rubio-Abadal, T. Yefsah, V. Khemani, D. A. Huse, I. Bloch, and C. Gross, Science **352**, 1547 (2016).

[12] C. R. Monroe, R. J. Schoelkopf, and M. D. Lukin, Sci. Am. **314**, 50 (2016).

[13] H. Bernien, S. Schwartz, A. Keesling, H. Levine, A. Omran, H. Pichler, S. Choi, A. S. Zibrov, M. Endres, M. Greiner *et al.*, Nature (London) **551**, 579 (2017).

[14] C. Neill, P. Roushan, K. Kechedzhi, S. Boixo, S. V. Isakov, V. Smelyanskiy, A. Megrant, B. Chiaro, A. Dunsworth, K. Arya *et al.*, Science **360**, 195 (2018).

[15] N. Y. Yao and C. Nayak, Phys. Today **71**(9), 40 (2018).

[16] H. Zhou, J. Choi, S. Choi, R. Landig, A. M. Douglas, J. Isoya, F. Jelezko, S. Onoda, H. Sumiya, P. Cappellaro, H. S. Knowles, H. Park, and M. D. Lukin, Phys. Rev. X **10**, 031003 (2020).

[17] Y. Sekino and L. Susskind, J. High Energy Phys. 10 (2008) 065.

[18] J. M. Maldacena, S. H. Shenker, and D. Stanford, J. High Energy Phys. 08 (2016) 106.

[19] A. I. Larkin and Y. N. Ovchinnikov, Sov. Phys. JETP **28**, 1200 (1969) [ZhETF **55**, 2262 (1969)].

[20] R. B. Laughlin, Nucl. Phys. B **2**, 213 (1987).

[21] A. Kitaev, in Brown Physics Colloquium, 2017, https://youtu.be/pFBAm7UCFHQ.

[22] P. R. Zangara, D. Bendersky, P. R. Levstein, and H. M. Pastawski, Phil. Trans. R. Soc. A **374**, 20150163 (2016).

[23] J. Kurchan, J. Stat. Phys. **171**, 965 (2018).

[24] M. Schleier-Smith, Nat. Phys. **13**, 724 (2017).

[25] B. Yan, L. Cincio, and W. H. Zurek, Phys. Rev. Lett. **124**, 160603 (2020).

[26] P. R. Levstein, G. Usaj, and H. M. Pastawski, J. Chem. Phys. **108**, 2718 (1998).

[27] R. A. Jalabert and H. M. Pastawski, Phys. Rev. Lett. **86**, 2490 (2001).

[28] A. Goussev, R. A. Jalabert, H. M. Pastawski, and D. A. Wisniacki, Scholarpedia **7**, 11687 (2012).

[29] I. L. Aleiner, L. Faoro, and L. B. Ioffe, Ann. Phys. (NY) **375**, 378 (2016).

[30] E. B. Rozenbaum, S. Ganeshan, and V. Galitski, Phys. Rev. Lett. **118**, 086801 (2017).

[31] J. Li, R. Fan, H. Wang, B. Ye, B. Zeng, H. Zhai, X. Peng, and J. Du, Phys. Rev. X **7**, 031011 (2017).

[32] R. J. Lewis-Swan, A. Safavi-Naini, J. J. Bollinger, and A. M. Rey, Nat. Commun. **10**, 1581 (2019).

[33] T. Goldfriend and J. Kurchan, Phys. Rev. E **102**, 022201 (2020).

[34] J. M. Maldacena, Nat. Rev. Phys. **2**, 123 (2020).

[35] J. Horgan, Sci. Am. (2020).

[36] P. W. Anderson, Rev. Mod. Phys. **50**, 191 (1978).

[37] P. W. Anderson, Science **177**, 393 (1972).

[38] P. R. Zangara and H. M. Pastawski, Phys. Scr. **92**, 033001 (2017).

[39] G. C. Ghirardi, A. Rimini, and T. Weber, Phys. Rev. D **34**, 470 (1986).

[40] S. Weinberg, Phys. Rev. A **85**, 062116 (2012).

[41] G. Feher, Phys. Rev. **114**, 1219 (1959).

[42] S. Sachdev, *Quantum Phase Transitions* (Cambridge University, New York, 2009).

[43] P. W. Anderson, J. Phys. Soc. Jpn. **9**, 316 (1954).

[44] H. T. Quan, Z. Song, X. F. Liu, P. Zanardi, and C. P. Sun, Phys. Rev. Lett. **96**, 140604 (2006).

[45] J. Zhang, X. Peng, N. Rajendran, and D. Suter, Phys. Rev. Lett. **100**, 100501 (2008).

[46] G. A. Álvarez, D. Suter, and R. Kaiser, Science **349**, 846 (2015).

[47] K. X. Wei, C. Ramanathan, and P. Cappellaro, Phys. Rev. Lett. **120**, 070501 (2018).

[48] P. C. Maurer, G. Kucsko, C. Latta, L. Jiang, N. Y. Yao, S. D. Bennett, F. Pastawski, D. Hunger, N. Chisholm, M. Markham, *et al.*, Science **336**, 1283 (2012).

[49] W. Zhang and D. G. Cory, Phys. Rev. Lett. **80**, 1324 (1998).

[50] G. S. Boutis, D. Greenbaum, H. Cho, D. G. Cory, and C. Ramanathan, Phys. Rev. Lett. **92**, 137201 (2004).

[51] E. Hahn, Phys. Rev. **80**, 580 (1950).

[52] R. G. Brewer and E. L. Hahn, Sci. Am. **251**, 50 (1984)

[53] W.-K. Rhim, A. Pines, and J. S. Waugh, Phys. Rev. B **3**, 684 (1971).

[54] M. Munowitz and A. Pines, Science **233**, 525 (1986).

[55] M. Niknam, L. F. Santos, and D. G. Cory, Phys. Rev. Research **2**, 013200 (2020).

[56] C. M. Sánchez, A. K. Chattah, K. X. Wei, L. Buljubasich, P. Cappellaro, and H. M. Pastawski, Phys. Rev. Lett. **124**, 030601 (2020).

[57] S. Zhang, B. H. Meier, and R. R. Ernst, Phys. Rev. Lett. **69**, 2149 (1992).

[58] G. Usaj, H. M. Pastawski, and P. R. Levstein, Mol. Phys. **95**, 1229 (1998).

[59] P. R. Levstein, A. K. Chattah, H. M. Pastawski, J. Raya, and J. Hirschinger, J. Chem. Phys. **121**, 7313 (2004).

[60] R. R. Ernst, 1996 (private communication).

[61] D. G. Cory, 1997 (private communication).

[62] H. M. Pastawski, P. R. Levstein, G. Usaj, J. Raya, and J. Hirschinger, Physica A **283**, 166 (2000).

[63] S. W. Morgan, V. Oganesyan, and G. S. Boutis, Phys. Rev. B **86**, 214410 (2012).

[64] C. M. Sánchez, L. Buljubasich, H. M. Pastawski, and A. K. Chattah, J. Magn. Reson. **281**, 75 (2017).

[65] W.-K. Rhim, A. Pines, and J. S. Waugh, Phys. Rev. Lett. **25**, 218 (1970).

[66] U. Haeberlen, *High Resolution NMR in Solids* (Academic, New York, 1976).

[67] T. Kuwahara, T. Mori, and K. Saito, Ann. Phys. (NY) **367**, 96 (2016).

[68] L. Buljubasich, C. M. Sánchez, A. D. Dente, P. R. Levstein, A. K. Chattah, and H. M. Pastawski, J. Chem. Phys. **143**, 164308 (2015).

[69] C. P. Slichter, *Principles of Magnetic Resonance* (Springer-Verlag, Berlin, 1990).

[70] R. R. Ernst, G. Bodenhausen, and A. Wokaun, *Principles of Nuclear Magnetic Resonance in One and Two Dimensions* (Oxford University, New York, 1987).

[71] C. M. Sánchez, P. R. Levstein, L. Buljubasich, H. M. Pastawski, and A. K. Chattah, Phil. Trans. R. Soc. A **374**, 20150155 (2016).

[72] A. Abragam, *Principles of Nuclear Magnetism* (Oxford University, New York, 2007).

[73] B. Yan and W. H. Zurek, arXiv:2110.09463 (2021).

[74] V. V. Flambaum and F. M. Izrailev, Phys. Rev. E **64**, 026124 (2001).

[75] W. H. Zurek, F. M. Cucchietti, and J. P. Paz, Acta Phys. Pol. B **38**, 1685 (2007).

[76] G. A. Álvarez, E. P. Danieli, P. R. Levstein, and H. M. Pastawski, J. Chem. Phys. **124**, 194507 (2006).

[77] H. M. Pastawski and G. Usaj, Phys. Rev. B **57**, 5017 (1998).

[78] D. G. Cory, A. F. Fahmy, and T. F. Havel, Proc. Natl. Acad. Sci. USA **94**, 1634 (1997).

[79] H. M. Pastawski, P. R. Levstein, and G. Usaj, Phys. Rev. Lett. **75**, 4310 (1995).

[80] H. Cho, T. D. Ladd, J. Baugh, D. G. Cory, and C. Ramanathan, Phys. Rev. B **72**, 054427 (2005).

[81] G. A. Alvarez, E. P. Danieli, P. R. Levstein, and H. M. Pastawski, Phys. Rev. A **82**, 012310 (2010).

[82] D. Bendersky, Ph.D. thesis, Universidad Nacional Córdoba, 2016.

[83] B. Swingle, Nat. Phys. **14**, 988 (2018).

[84] F. Lozano-Negro, P. R. Zangara, and H. M. Pastawski, Chaos, Solitons Fractals **150**, 111175 (2021).

[85] A. K. Khitrin, Chem. Phys. Lett. **274**, 217 (1997).

[86] M. Munowitz, A. Pines, and M. Mehring, J. Chem. Phys. **86**, 3172 (1987).

[87] B. Yoshida and N. Y. Yao, Phys. Rev. X **9**, 011006 (2019).

[88] F. D. Domínguez, M. C. Rodríguez, R. Kaiser, D. Suter, and G. A. Álvarez, Phys. Rev. A **104**, 012402 (2021).

[89] V. E. Zobov and A. A. Lundin, Appl. Magn. Reson. (2021).

[90] I. L. Aleiner and A. I. Larkin, Phys. Rev. B **54**, 14423 (1996).

[91] F. M. Cucchietti, H. M. Pastawski, and R. A. Jalabert, Phys. Rev. B **70**, 035311 (2004) (see Figs. 4–6).

[92] G. Casati, B. Chirikov, D. Shepelyansky, and I. Guarnieri, Phys. Rep. **154**, 77 (1987).

[93] T. A. Elsayed and B. V. Fine, Phys. Scr. **T165**, 014011 (2015).

[94] P. Jacquod, P. G. Silvestrov, and C. W. J. Beenakker, Phys. Rev. E **64**, 055203(R) (2001).

[95] P. Jacquod, I. Adagideli, and C. W. J. Beenakker, Phys. Rev. Lett. **89**, 154103 (2002).

[96] P. van Ede van der Pals and P. Gaspard, Phys. Rev. E **49**, 79 (1994).

[97] D. Jyoti, M.Sc. thesis, Dartmouth College, 2017, arXiv:1711.01948.

[98] E. Rufeil-Fiori, C. M. Sánchez, F. Y. Oliva, H. M. Pastawski, and P. R. Levstein, Phys. Rev. A **79**, 032324 (2009).

[99] J. Orban and A. Bellemans, Phys. Lett. A **24**, 620 (1967).

[100] R. Pinto, E. Medina, and H. M. Pastawski, BAPS March Meeting **2004**, J22.001 (2004).

[101] G. Manfredi and P.-A. Hervieux, Phys. Rev. Lett. **100**, 050405 (2008).

[102] L. J. Fernández-Alcázar and H. M. Pastawski, Phys. Rev. A **91**, 022117 (2015).

[103] C. M. Sánchez, H. M. Pastawski, and P. R. Levstein, Physica B: Condensed Matter **398**, 472 (2007).

[104] H. M. Pastawski, G. Usaj, and P. R. Levstein, Chem. Phys. Lett. **261**, 329 (1996).

[105] Z. Mádi, B. Brutscher, T. Schulte-Herbrüggen, R. Brüschweiler, and R. Ernst, Chem. Phys. Lett. **268**, 300 (1997).

[106] P. Cappellaro, L. Viola, and C. Ramanathan, Phys. Rev. A **83**, 032304 (2011).

[107] F. M. Pastawski, B. Yoshida, D. Harlow, and J. Preskill, J. High Energy Phys. 06 (2015) 149.

[108] J. Horgan, Sci. Am. (2021).

[109] B. Yan and N. A. Sinitsyn, Phys. Rev. Lett. **125**, 040605 (2020).

[110] N. A. Sinitsyn and B. Yan, Sci. Am. (2020).

[111] A. Trabesinger, Nat. Phys. **8**, 263 (2012).

[112] I. M. Georgescu, S. Ashhab, and F. Nori, Rev. Mod. Phys. **86**, 153 (2014).